Experimental validation of an Actor-Critic Model Predictive Force Controller for robot-environment interaction tasks

Alessandro Pozzi [1], Luca Puricelli [1], Vincenzo Petrone [2], Enrico Ferrentino [1], Pasquale Chiacchio [1], Francesco Braghin [1], and Loris Roveda [1]

[1]Affiliation not available
[2]University of Salerno

October 31, 2023

Abstract

In industrial settings, robots are typically employed to accurately track a reference force to exert on the surrounding environment to complete interaction tasks.

Interaction controllers are typically used to achieve this goal. Still, they either require manual tuning, which demands a significant amount of time, or exact modeling of the environment the robot will interact with, thus possibly failing during the actual application.

A significant advancement in this area would be a high-performance force controller that does not need operator calibration and is quick to be deployed in any scenario.

With this aim, this paper proposes an **A**ctor-**C**ritic **M**odel **P**redictive **F**orce **C**ontroller (**ACMPFC**), which outputs the optimal setpoint to follow in order to guarantee force tracking, computed by continuously trained neural networks.

This strategy is an extension of a reinforcement learning-based one, born in the context of human-robot collaboration, suitably adapted to robot-environment interaction.

We validate the ACMPFC in a real-case scenario featuring a Franka Emika Panda robot.

Compared with a base force controller and a learning-based approach, the proposed controller yields a reduction of the force tracking MSE, attaining fast convergence: with respect to the base force controller, ACMPFC reduces the MSE by a factor of 4.35.

Experimental validation of an Actor-Critic Model Predictive Force Controller for robot-environment interaction tasks

Alessandro Pozzi[1][a], Luca Puricelli[1][b], Vincenzo Petrone[2][c], Enrico Ferrentino[2][d], Pasquale Chiacchio[2][e], Francesco Braghin[1][f] and Loris Roveda[3][g]

[1]*Department of Mechanical Engineering, Politecnico di Milano, 20133 Milano, Italy*

[2]*Department of Computer Engineering, Electrical Engineering and Applied Mathematics (DIEM), University of Salerno, 84084 Fisciano, Italy*

[3]*Istituto Dalle Molle di Studi sull'Intelligenza Artificiale (IDSIA), Scuola Universitaria Professionale della Svizzera Italiana (SUPSI), Università della Svizzera Italiana (USI), 6962 Lugano, Switzerland*

{ *alessandro11.pozzi, luca.puricelli* }*@mail.polimi.it,* { *vipetrone, eferrentino, pchiacchio* }*@unisa.it, francesco.braghin@polimi.it, loris.roveda@idsia.ch*

This work has been accepted for publication at ICINCO 2023 - 20th International Conference on Informatics in Control, Automation and Robotics on Monday 31st July, 2023.

Keywords: Physical Robot-Environment Interaction, Artificial Neural Networks, Optimized Interaction Control, Impedance Control

Abstract: In industrial settings, robots are typically employed to accurately track a reference force to exert on the surrounding environment to complete interaction tasks. Interaction controllers are typically used to achieve this goal. Still, they either require manual tuning, which demands a significant amount of time, or exact modeling of the environment the robot will interact with, thus possibly failing during the actual application. A significant advancement in this area would be a high-performance force controller that does not need operator calibration and is quick to be deployed in any scenario. With this aim, this paper proposes an Actor-Critic Model Predictive Force Controller (ACMPFC), which outputs the optimal setpoint to follow in order to guarantee force tracking, computed by continuously trained neural networks. This strategy is an extension of a reinforcement learning-based one, born in the context of human-robot collaboration, suitably adapted to robot-environment interaction. We validate the ACMPFC in a real-case scenario featuring a Franka Emika Panda robot. Compared with a base force controller and a learning-based approach, the proposed controller yields a reduction of the force tracking MSE, attaining fast convergence: with respect to the base force controller, ACMPFC reduces the MSE by a factor of 4.35.

1 INTRODUCTION

1.1 Context

Most of nowadays manufacturing processes require the massive employment of robots. Industries are increasingly deploying manipulators in their production processes to accomplish interaction tasks like polishing, deburring, or assembly, with the aim of increasing the levels of quality and customization of the delivered products.

Given the wide range of practical scenarios manipulators are employed in, robot control is one of the major interests of the current scientific research, especially in the industrial sector. In order to accommodate the propensity of manufacturers to improve the cost, accuracy and throughput of their production plants, in the last decades researchers have proposed a vast spectrum of advantageous alternatives to classical control techniques like the well-known and largely used linear PID controllers.

Optimal control is among the most consolidated

[a] https://orcid.org/0000-0002-6460-4669
[b] https://orcid.org/0000-0003-1736-0822
[c] https://orcid.org/0000-0003-4777-1761
[d] https://orcid.org/0000-0003-0768-8541
[e] https://orcid.org/0000-0003-3385-8866
[f] https://orcid.org/0000-0002-0476-4118
[g] https://orcid.org/0000-0002-4427-536X

disciplines in advanced control, given its capability of explicitly optimizing a certain objective function, appropriately parameterized to maximize desired performance indices, according to the task requirements. Generally speaking, the fields of application of optimal control frameworks cover a broad variety of scenarios: in principle, they are suitable to optimize any system formulated as a dynamic model, from simple linear integrators (Preitl et al., 2006) to complex biological systems (Rigatos et al., 2016).

In robotics, one can benefit from optimizing numerous quantities, e.g. trajectory tracking or joint vibration (Mohd Hanif et al., 2021), to ensure accuracy in the performed task. This fundamental problem can be addressed with various approaches, such as fractional-order control (Ataşlar-Ayyıldız, 2023) or double PID controllers to manage both motor position and velocity (Ucgun et al., 2022). Another popular technique in this context is fuzzy logic control, used to improve the system stability, rise time, and steady-state error (Obadina et al., 2022). Furthermore, exploiting optimization algorithms like spiral dynamics algorithms (Kasruddin Nasir et al., 2021) and particle swarm optimization (Sathish Kumar et al., 2023), fuzzy logic controllers can be optimally tuned to tackle trajectory and velocity tracking (Liu et al., 2022).

1.2 Related Works

Trajectory-tracking accuracy is not the only performance roboticists aim at optimizing: indeed, one fundamental feature to control, particularly in industrial applications, is robot-environment interaction. To this aim, interaction controllers are adopted to guarantee stability and safety of the working environment while accurately tracking precise force profiles, so as to maximize the production quality.

Delivering the aforementioned characteristics is the core objective of interaction controllers: the pioneering work in (Mason, 1981) set off the divisions of interaction control strategies into two macro-categories: direct force control (Khatib, 1987) and impedance control (Hogan, 1984), with the latter being typically preferred to the former for its capability of inherently providing the manipulator with a compliant behavior. Unfortunately, impedance controllers lack accurate force tracking, a feature requiring, as demonstrated in (Jung et al., 2004), a complete and exact characterization of the environment, which is, in general, a utopian intent to accomplish.

Therefore, impedance controllers with force-tracking capabilities have been widely addressed in literature with various strategies, from variable impedance (Jung et al., 2004; Duan et al., 2018; Roveda et al., 2020; Shu et al., 2021) or variable stiffness (Lee and Buss, 2008) techniques to reference generation methods (Seraji and Colbaugh, 1997; Liang et al., 2018; Roveda et al., 2020; Li et al., 2023): recently, (Roveda and Piga, 2021) proposed using a PI direct force control law as reference generator for an inner-loop impedance controller.

Learning methods are specifically suitable for robot-environment interaction tasks: these optimization-based approaches are indeed a powerful tool to learn unmodeled effects that can influence the dynamics of the controlled plant, overcoming the main limitation of the abovementioned standard techniques, i.e. the human effort in tuning the additional parameters needed by the introduced force control law. For this reason, researchers are currently focusing on applying AI-based strategies on impedance controllers for parameter tuning (Zhang et al., 2021) or residual action computation (Johannink et al., 2019; Puricelli et al., 2023). Other common approaches are exploiting neural networks to estimate the human-robot (Roveda et al., 2022) or robot-environment (Peng et al., 2021) interaction dynamics, or adopting reinforcement learning (Johannink et al., 2019; Roveda et al., 2022) to optimize a certain task. Most of them are task-specific, e.g. (Zhang et al., 2021), and require a considerable amount of trials (or simulation-to-real transfer) to reach optimal performance (Johannink et al., 2019).

1.3 Contribution

This paper proposes an Actor-Critic Model Predictive Force Controller (ACMPFC) capable of providing force-tracking capabilities to a low-level impedance controller. The ACMPFC is composed of two control loops: the outer loop (which we also term *high-level controller*) computes a setpoint for the inner-loop impedance controller to accurately follow a desired force reference.

The high-level control strategy makes use of a Reinforcement Learning (RL) approach, previously used for physical human-robot collaboration (Roveda et al., 2022): the contribution of this work is hence to demonstrate how such a technique can be adapted for robot-environment interaction tasks, guaranteeing precise force tracking. This feature is fundamental in several practical use-cases, e.g. welding, cutting or polishing, for which our method delivers better performance compared to standard controllers.

We have discussed in Sections 1.1 and 1.2 that optimal control and learning control are paramount for improving the performance of robot-environment interaction controllers. Therefore, motivated by the discussed necessities, our method exploits both frameworks. Indeed, the ACMPFC makes uses of Neural Networks (NNs) for a two-fold objective: (i) forming a Model Approximator (MA), used for estimating the interaction dynamics, and (ii) developing an Actor-Critic strategy for the computation of the optimal setpoint to track.

We show that ACMPFC can reduce the force-tracking error when compared to both a general-purpose PI Force Controller (PIFC) (Roveda and Piga, 2021) and a different AI-based optimal controller, known as ORACLE (Puricelli et al., 2023). In particular, ACMPFC outperforms PIFC in terms of tracking accuracy, and, at the same time, it overcomes the main disadvantage of ORACLE, which is a consistent time delay in exerting the desired force profile. All the experiments are run on a real manipulator, i.e. the Franka Emika's Panda robot shown in Figure 1, whose kinematic structure consists of 7 serial revolute joints.

The remainder of this article is structured as follows. Section 2 elaborates on the design of the proposed methodology, whereas Section 3 presents the results obtained by its employment; Section 4 concludes the paper, discussing on the attained achievements and briefly presenting possible future developments.

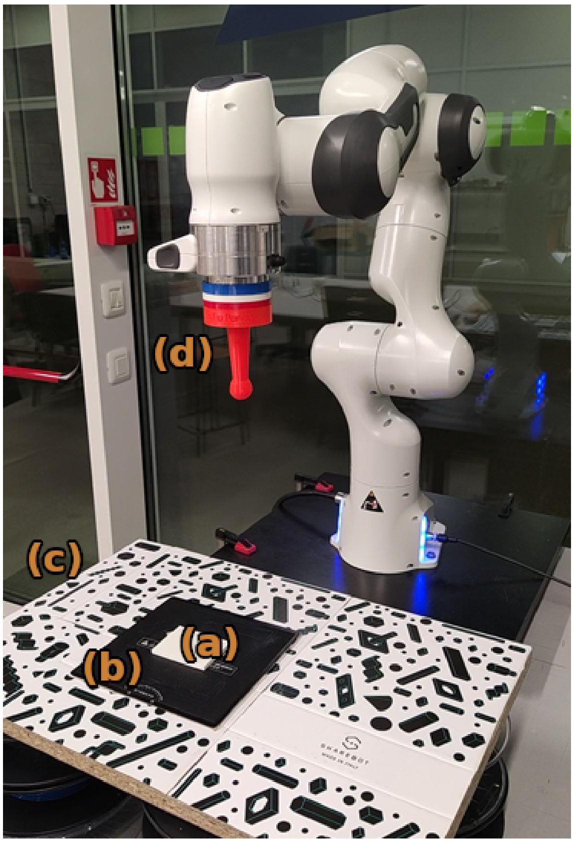

Figure 1: Real scenario testing bench. It features a Franka Emika's Panda robot coming into contact with the environment, represented by the white thin block (a) rigidly attached to a larger surface (b) that slides over the plane (c). This particular configuration reduces stick-slip effects during the interaction. The 3D-printed spherical end-effector (d) provides a small interaction surface with the material, making it possible to model the contact with the environment as a spring in the exploration phase (i.e. the phase during which the Actor's bounds are computed, as mentioned in Section 2.3.4).

2 METHODOLOGY

The ACMPFC is a RL-based strategy that provides enhanced force-tracking capabilities to an impedance controller. Given a desired wrench to exert on the environment, it provides the underlying impedance controller, not able to follow the reference wrench by itself, with the correct setpoint to track. The whole architecture, illustrated in the diagram of Figure 2, consists of the following components: (i) an inner-loop impedance controller, that ensures a stable compliant behavior with respect to the environment; (ii) three Feed-Forward Neural Networks (FFNNs) that, by cooperation, constitute the outer-loop controller, computing the optimal setpoint for the low-level impedance controller; (iii) data storage, including the trajectories to execute to train the ACMPFC over the episodes. All these components are described in detail in the next sections.

2.1 Impedance Controller

In order to be able to compare the ACMPFC with the control architectures in (Roveda and Piga, 2021; Puricelli et al., 2023), it is necessary to adopt the same low-level impedance controller. This inner-loop controller imposes the desired compliance on the robot's end-effector (EE) while controlling a setpoint pose, that will be provided in advance by the outer-loop reference generator.

A manipulator robot with n Degrees of Freedom (DOFs), performing an m-dimensional task, with $m \leq 6 \leq n$, can be described by the following dynamic model:

$$\boldsymbol{M}(\boldsymbol{q})\ddot{\boldsymbol{q}} + \boldsymbol{C}(\boldsymbol{q},\dot{\boldsymbol{q}})\dot{\boldsymbol{q}} + \boldsymbol{\tau}_f(\dot{\boldsymbol{q}}) + \boldsymbol{g}(\boldsymbol{q}) = \boldsymbol{\tau}_c - \boldsymbol{J}^T(\boldsymbol{q})\boldsymbol{f}_e,$$

where $\boldsymbol{M}(\boldsymbol{q}) \in \mathbb{R}^{n\times n}$ is the manipulator's inertia matrix, $\boldsymbol{C}(\boldsymbol{q},\dot{\boldsymbol{q}}) \in \mathbb{R}^{n\times n}$ is the matrix accounting for the Coriolis and centrifugal effects, $\boldsymbol{\tau}_f(\dot{\boldsymbol{q}}) \in \mathbb{R}^{n\times 1}$ accounts for static and viscous friction, $\boldsymbol{g}(\boldsymbol{q}) \in \mathbb{R}^{n\times 1}$ represents the torque exerted on the links by grav-

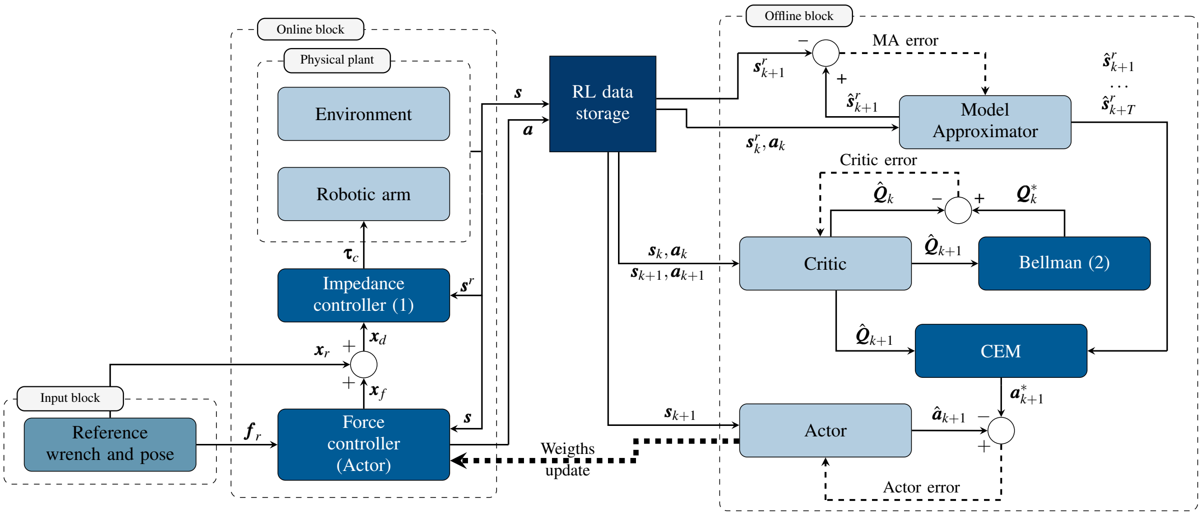

Figure 2: ACMPFC functioning scheme. The RL data storage includes the system's states and actions over the execution of a trajectory, and forwards them to the NNs for off-line training between consecutive episodes.

ity, $\boldsymbol{\tau}_c \in \mathbb{R}^{n\times 1}$ indicates the impedance control action, $\boldsymbol{J}(\boldsymbol{q}) \in \mathbb{R}^{m\times n}$ is the geometric Jacobian, $\boldsymbol{f}_e \in \mathbb{R}^{m\times 1}$ is the vector of wrenches exerted by the robot end-effector (EE) on the environment. The vectors $\boldsymbol{q}, \dot{\boldsymbol{q}}, \ddot{\boldsymbol{q}} \in \mathbb{R}^{n\times 1}$ represent positions, velocities, and accelerations of the manipulator's joints, respectively.

The impedance control law with robot dynamics compensation can be written as (Formenti et al., 2022):

$$\boldsymbol{\tau}_c = \boldsymbol{J}^T(\boldsymbol{q})\boldsymbol{f}_c + \boldsymbol{C}(\boldsymbol{q},\dot{\boldsymbol{q}})\dot{\boldsymbol{q}} + \boldsymbol{g}(\boldsymbol{q}), \tag{1}$$

with

$$\begin{aligned}\boldsymbol{f}_c =& \boldsymbol{M}_x(\boldsymbol{q})\ddot{\boldsymbol{x}}_d - \boldsymbol{f}_e + \\ & \boldsymbol{M}_x(\boldsymbol{q})\boldsymbol{M}_{imp}^{-1}\left(\boldsymbol{f}_e - \boldsymbol{K}_{imp}\Delta\boldsymbol{x} - \boldsymbol{D}_{imp}\Delta\dot{\boldsymbol{x}}\right),\end{aligned}$$

where $\boldsymbol{M}_x(\boldsymbol{q}) \triangleq \left(\boldsymbol{J}^T(\boldsymbol{q})\right)^{\dagger}\boldsymbol{M}(\boldsymbol{q})\left(\boldsymbol{J}(\boldsymbol{q})\right)^{\dagger} \in \mathbb{R}^{m\times m}$ is the task-space inertia matrix, with $(\cdot)^{\dagger}$ indicating the pseudo-inverse matrix. $\Delta\boldsymbol{x} \triangleq \boldsymbol{x}_d - \boldsymbol{x}$ is the error between the desired EE pose $\boldsymbol{x}_d$ and the actual pose $\boldsymbol{x}$. With $m = 6$, $\boldsymbol{x} = (x, y, z, \phi, \vartheta, \psi)^T$ represents the full robot EE pose, composed of position (x, y, z) and orientation (ϕ, ϑ, ψ). $\Delta\dot{\boldsymbol{x}} \triangleq \dot{\boldsymbol{x}}_d - \dot{\boldsymbol{x}}$ represents the pose error derivative. $\boldsymbol{M}_{imp}, \boldsymbol{D}_{imp}, \boldsymbol{K}_{imp} \in \mathbb{R}^{m\times m}$ are the impedance control parameters (i.e., mass, damping, and stiffness diagonal matrices, respectively), which can be tuned, in accordance to the rules in (Roveda and Piga, 2021), to ensure a medium-soft robot-environment interaction and a bandwidth of 2.5 Hz. Typically, the coefficients of $\boldsymbol{D}_{imp}$ are chosen as $d_{imp,i} = 2\xi_i\sqrt{m_{imp,i}k_{imp,i}}$, with ξ_i being the damping ratio and $i = 1, 2, \ldots, m$ is the axis index.

2.2 Control Architecture

The high-level controller relies on an Actor-Critic structure, a RL technique consisting of an agent interacting with an environment with the goal of optimizing the reward received by performing actions on it. The system to be controlled is modeled as a Markov Decision Process (MDP) (Bellman, 1958), i.e. it is represented as a tuple $\langle \mathcal{S}, \mathcal{A}, P, R, \lambda \rangle$, where $\mathcal{S}$ represents the finite set of the system's states, $\mathcal{A}$ is the finite set of actions the actor can execute, $P(s_{k+1} \mid s_k, a_k)$ is the state transition probability matrix from state s_k to state s_{k+1} by taking the action a_k, $R(s,a) = \mathbb{E}\left[r \mid s, a\right]$ is the reward function outputting the expectation of the reward r obtained from the environment at state s if the agent's action is a, and $\lambda \in [0;1]$ is the discount factor.

Depending on the environment configuration, the task objective, and the semantics of the reward function, the optimization problem can be stated as either maximization or minimization of the reward function. In the latter case, the reward function can be interpreted, without loss of generality, as a *cost function*. Henceforth, we will use the term “reward function” for convenience.

As a RL algorithm, the ACMPFC's goal is to find the optimal control policy $\pi^*(a \mid s)$, which optimizes the cumulative reward, by continuously interacting with the environment. The components of the Actor-Critic strategy are (i) the *Actor*, i.e. the agent that applies actions on the environment, modifying its state and receiving rewards; (ii) the *Critic*, i.e. the entity that establishes the value of actions taken by the actor, given the predicted evolution of the system.

In our case, the system to be controlled is the robot-environment physical plant: its state is defined as $\boldsymbol{s} = (\boldsymbol{x}, \dot{\boldsymbol{x}}, \boldsymbol{f}_e, \boldsymbol{\Delta f})$, while the action is the control variable $\boldsymbol{a} = \boldsymbol{x}_f$, whose tracking minimizes the force error $\Delta \boldsymbol{f} \triangleq \boldsymbol{f}_r - \boldsymbol{f}_e$, where $\boldsymbol{f}_r$ is the force reference to exert on the environment, specified by the task requirements.

In brief, the controller design is led by the following optimization problem:

$$\boldsymbol{x}_f = \arg\min \{\boldsymbol{R}(\boldsymbol{\Delta}\tilde{\boldsymbol{f}})\},$$

where $\boldsymbol{R}(\boldsymbol{\Delta}\tilde{\boldsymbol{f}})$ is the reward function, which will be formalized later. Note that its argument is the *expected* force error $\boldsymbol{\Delta}\tilde{\boldsymbol{f}} \triangleq \boldsymbol{f}_r - \tilde{\boldsymbol{f}}_e$, which depends on the expected interaction force $\tilde{\boldsymbol{f}}_e$. The actual interaction force $\boldsymbol{f}_e$ is unknown because it strictly depends on the environment, and is known by the agent through measurements only after the control action $\boldsymbol{x}_f$ is applied and the next state is observed.

Here follows a brief explanation of the entities involved in the ACMPFC; additional implementation details, together with a proof of convergence of the RL-based algorithm, can be found in (Roveda et al., 2022).

2.2.1 Actor

The Actor computes the action $\hat{\boldsymbol{a}}$ to be taken at state $\boldsymbol{s}$, with a FFNN approximating the optimal policy $\pi^*(\boldsymbol{a} \mid \boldsymbol{s})$. By minimizing the MSE with respect to the optimal action $\boldsymbol{a}^*$, computed by the Critic via the Cross-Entropy Method (which will be explained next), the learning process will make the Actor's actual policy $\hat{\pi}$ tend to the optimal policy π^*.

More specifically, the Actor's NN is trained in agreement with the following optimization problem:

$$\min_{\theta^A} \sum_{i=0}^{m} \left(\boldsymbol{a}_i^* - \hat{\boldsymbol{a}}_i(\theta^A)\right)^2,$$

with the NN parameters θ^A updated applying a Stochastic Gradient Descent (SGD) optimization.

2.2.2 Critic

The Critic assesses the value of the Actor's policy by approximating the action-value function (also called Q-function) $Q^{\pi}(s,a)$, returning the value associated with taking a particular action a in the state s, implemented with a FFNN. Let $\hat{\boldsymbol{Q}}_k \triangleq \hat{\boldsymbol{Q}}(\boldsymbol{s}_k, \boldsymbol{a}_k)$ be the output of the Critic at time k, computing a different value for each control direction. The Critic's NN learning goal is minimizing the MSE with respect to the optimal Q-value $\boldsymbol{Q}^*$, computed according to Bellman's equation (Bellman, 1952):

$$\boldsymbol{Q}_k^* = \boldsymbol{R}_k + \lambda \hat{\boldsymbol{Q}}_{k+1}, \tag{2}$$

where $\boldsymbol{Q}_k^* \triangleq \boldsymbol{Q}^*(\boldsymbol{s}_k, \boldsymbol{a}_k)$ and $\boldsymbol{R}_k \triangleq \boldsymbol{R}(\boldsymbol{s}_k, \boldsymbol{a}_k)$.

More formally, the minimization problem yielding the Critic's NN's training is the following:

$$\min_{\theta^C} \sum_{i=0}^{m} \left(\boldsymbol{Q}_i^* - \hat{\boldsymbol{Q}}_i(\theta^C)\right)^2,$$

with the NN parameters θ^C updated applying a SGD optimization.

It is now worth discussing how our architecture compares to other common Actor-Critic structures, i.e. DDPG (Lillicrap et al., 2015), SAC (Haarnoja et al., 2018) and TD3 (Fujimoto et al., 2018). The most immediate aspect to highlight is that our architecture foresees a *single* NN to implement the Critic, whereas both SAC and TD3 require two Critic networks to explicitly leverage the problem of maximization bias, with the former employing an additional value network to compute the Q-value. On the other hand, DDPG uses a single network, similarly to our controller: the only difference is that DDPG exploits two additional NNs, namely the *target* Actor and Critic networks, used to compute the target Q-value $\boldsymbol{Q}^*$ needed to train the Critic, while in our architecture it is computed with the Bellman equation in (2).

2.2.3 Cross-Entropy Method

The Cross-Entropy Method (CEM) (de Boer et al., 2005) computes the optimal action $\boldsymbol{a}^*$ so as to maximize the cumulative reward over a prediction horizon T, computed by making inference on the Critic, in fact implementing a Model Predictive Control (MPC) strategy. The future states $\{\boldsymbol{s}_i\}_{i=k+1}^{k+T}$ are inferred from the Model Approximator (MA).

The strategy of the algorithm is to sample the action space, approximating the distributions of suitable solutions, assumed to be, e.g., Gaussian. Sampling from these distributions generates possible candidate sequences of solutions. The distributions are iteratively updated on the basis of the *best* candidate sequences, i.e., in our case, the ones maximizing the cumulative reward. As the algorithm progresses, the distributions become more and more refined, until convergence to optimal solutions. The pseudo-code describing its implementation is given in Algorithm 1.

The reader should note that the CEM algorithm overcomes the problem of overestimation bias, which is one of the main issues with most Deep Actor-Critic RL methods. Indeed, by randomly sampling sequences of actions/states and updating the stochastic distributions' parameters according to the best sequences, the Actor is less influenced by the inherent bias of explicitly selecting the action that optimizes the Q-value computed by only one Critic.

Data: current state $\boldsymbol{s}_k$ from the RL data storage
Parameters: T, N_{it}, $N_{samples}$, N_{elites}, α
Result: optimal control action $\boldsymbol{a}^*$
initialize the mean μ and the standard deviation σ of the T stochastic distributions $\{\mathcal{D}_t \sim \mathcal{N}(\mu_t, \sigma_t)\}_{t=0}^{T-1}$;
for $iter = 1, 2, \ldots, N_{it}$ **do**
  for $j = 1, 2, \ldots, N_{samples}$ **do**
    sample a random sequence of actions $\{\boldsymbol{a}_t^j\}_{t=0}^{T-1}$ from $\mathcal{D}_t$;
    predict the system evolution through the MA: $\{\boldsymbol{s}_t^j\}_{t=1}^{T-1}$, with $\boldsymbol{s}_0^j := \boldsymbol{s}_k$;
    evaluate the cumulative reward as $\mathrm{r}_j = \sum_{t=0}^{T-1} \boldsymbol{R}_t^j + \hat{\boldsymbol{Q}}_{T-1}^j$;
  end
  sort the sequences $\boldsymbol{a}^j$ with respect to r_j in increasing order;
  let $\boldsymbol{a}^{elites}$ be the best N_{elites} sequences;
  for $t = 0, 1, \ldots, T-1$ **do**
    compute mean μ_t^{elites} and standard deviation σ_t^{elites} of $\boldsymbol{a}_t^{elites}$;
    update $\mu_t \leftarrow (1-\alpha)\mu_t + \alpha\mu_t^{elites}$;
    update $\sigma_t \leftarrow (1-\alpha)\sigma_t + \alpha\sigma_t^{elites}$;
    update $\mathcal{D}_t$ with the new values of μ_t and σ_t;
  end
end

Algorithm 1: Cross-Entropy Method (CEM)

2.2.4 Model Approximator

The Model Approximator estimates the robot-environment system's dynamics; thus, it considers the reduced state $\boldsymbol{s}^r \triangleq (\boldsymbol{x}, \dot{\boldsymbol{x}}, \boldsymbol{f}_e)$ and its evolution over time, as the state variable $\boldsymbol{\Delta f}$ is not related to its actual dynamics. In particular, it embeds the transition of the system between two consecutive states, i.e. $\hat{\boldsymbol{s}}_{k+1}^r = \boldsymbol{s}_k^r + \boldsymbol{\delta\hat{s}}\left(\boldsymbol{s}_k^r, \boldsymbol{a}_k\right)$, under action $\boldsymbol{a}_k$, where $\boldsymbol{\delta\hat{s}}$ is the MA's output (Nagabandi et al., 2018), computed by an ensemble of FFNNs (Chua et al., 2018) at each time step k. It is exploited by the CEM to propagate the system's state over time, hence predicting its evolution.

Thanks to the NN ensemble, the MA allows for a data-efficient learning, as demonstrated in (Chua et al., 2018). Opting for different architectures, e.g. a single FFNN, would result in a less efficient training, thus requiring either more data or a different learning process, as in (Nagabandi et al., 2018).

The training procedure aims at minimizing the MSE with respect to the actual state $\boldsymbol{s}^r$, recorded during the execution of an episode, according to the following minimization problem:

$$\min_{\theta^{MA}} \sum_{i=0}^{m} \left(\boldsymbol{s}_i^r - \hat{\boldsymbol{s}}_i^r\left(\theta^{MA}\right)\right)^2,$$

with the NN parameters θ^{MA} updated applying a SGD optimization.

2.3 Learning Procedure

The control architecture described in Section 2.2 was originally developed and employed in the Q-Learning-based Model Predictive Variable Impedance Controller (QLMPVIC) (Roveda et al., 2022), instantiated for a Human-Robot Collaboration (HRC) scenario. Therein, an online learning strategy for the NNs is implemented: the high-level control loop frequency is set to 6 Hz and every 5 control steps, whose data are collected in the buffer, the training is performed and the networks' weights are updated. With respect to the work in (Roveda et al., 2022), several modifications are needed to adapt the learning procedure to a robot-environment scenario.

2.3.1 Offline Reinforcement Learning

The training of the NNs is performed offline, i.e. between two consecutive episodes. This allows the ACMPFC to work at 1 kHz since, as shown in Figure 2, during the online phase, the Actor's weights are fixed, and its NN is only used to infer the control action $\boldsymbol{x}_f$. During the episode execution, the system's states and the controller actions are stored in the buffer, and used in the next episode. This modification is crucial for the robot-environment interaction problem, as the controller must work at the robot's control frequency in order to properly manage the interaction forces.

2.3.2 Reward Function

In (Roveda et al., 2022), the objective is minimizing the exerted wrench $\boldsymbol{f}_e$, so as to make the human interaction as comfortable as possible. So, we introduce a modification in the reward function in order to properly pursue the objective of force tracking. In our case, the reward function is hence the following:

$$\boldsymbol{R}_k = \boldsymbol{c}_0 \cdot |\boldsymbol{f}_r(k) - \boldsymbol{f}_e(k)| + \boldsymbol{c}_1 \cdot |\boldsymbol{x}_f(k) - \boldsymbol{x}_f(k-1)|, \tag{3}$$

where the term $|\boldsymbol{f}_r(k) - \boldsymbol{f}_e(k)|$ is needed for force tracking purposes, whereas the term $|\boldsymbol{x}_f(k) - \boldsymbol{x}_f(k-1)|$ is needed to reduce overshoot or excessive variations of the desired set point $\boldsymbol{x}_f$, with operator '$\cdot$' indicating the element-wise product between vectors. The coefficients in $\boldsymbol{c}_0$ and $\boldsymbol{c}_1$ balance the trade-off between these relative contributions and must be selected by the user.

2.3.3 Impedance Control Setpoint

The hybrid force/position control law that generates the setpoint for the impedance controller can be written as follows:

$$\boldsymbol{x}_d = (\boldsymbol{I} - \boldsymbol{\Gamma})\boldsymbol{x}_r + \boldsymbol{\Gamma}\boldsymbol{x}_f,$$

where $\boldsymbol{x}_r$ is the reference pose, $\boldsymbol{I} \in \mathbb{R}^{m \times m}$ is the identity matrix, and, assuming the common case in which $m = 6$, $\boldsymbol{\Gamma} \triangleq \operatorname{diag}\left(\gamma_x, \gamma_y, \gamma_z, \gamma_\phi, \gamma_\vartheta, \gamma_\psi\right)$ is the task specification matrix (Khatib, 1987), with $\gamma_i = 1$ if the $i-$th direction is subject to force control, 0 otherwise.

2.3.4 Actor's Action Space Bounds

Since the controller must always guarantee the safety of both the robot structure and the working environment, the Actor's control action must be limited to a fixed range. The bounds of this range, as well as the environment's rest position $\boldsymbol{x}_e$, can be retrieved in a preliminary phase, in which the ACMPFC is deactivated, with only the impedance controller running. During this phase, the robot slowly approaches the environment, until a force threshold is registered. The lower bound on $\boldsymbol{x}_f$ is set to the position at which $\boldsymbol{x}_e$ is reached, while the upper bound is set to the position at which the force threshold is measured.

2.3.5 Contact Position Information Embedment

The last modification applied to the Q-LMPVIC comes consequently to the change of use case. Indeed, a problem occurs when feeding the NNs with the data as collected during training: $\boldsymbol{x}$ represents an absolute pose, so if the position of the environment changes, even slightly, from episode to episode, the NNs are not able to account for it. Therefore, we process the data before the training process, to make all poses relative. Consider, for instance, the case where the force reference has to be tracked along the z direction. The resultant Δz position that will be fed to the NNs will be $\Delta z \triangleq z - z_e$. Instead of feeding the robot's EE z coordinate directly, subtracting the environment position z_e allows making the NNs training and execution independent of the contact position and dealing only with penetrations.

3 RESULTS

We employ the proposed control approach on a real scenario, after first testing it in simulation. The real robot test is shown in the attached video[1]. The GitHub source code[2] makes it possible, for interested users, to reproduce our simulation and test it on new trajectories.

3.1 Task Setup and Materials

Both in simulation and real environments, the ACMPFC strategy is tested on a Franka Emika's Panda robot, a 7-DOF robotic arm. This platform exposes an interface to retrieve, via software, estimations of $\boldsymbol{f}_e$ from joint torque measurements. Alternatively, one can use flange-mounted force/torque sensors. The simulation tests are performed in MuJoCo (Todorov et al., 2012) for a realistic representation of the real-case scenario. The task consists of moving the EE, with a fixed orientation, along a planar trajectory, so as to exert a force normal (i.e. along the z axis) to the xy plane, also termed *contact surface*, i.e. $\boldsymbol{\Gamma} = \operatorname{diag}(0, 0, 1, 0, 0, 0)$.

Novel force control techniques are typically validated by assessing their performance, in terms of force-tracking error, against specific 1-dimensional force profiles, e.g. constants (Seraji and Colbaugh, 1997; Jung et al., 2004; Liang et al., 2018; Roveda et al., 2020; Li et al., 2023), step functions (Iskandar et al., 2023), or sine waves with periods in the order of seconds (Duan et al., 2018; Shu et al., 2021).

In our scenarios, the manipulator is asked to learn to track a mixed force reference, consisting of three subsequent sections: a ramp from 25 N to 35 N, a constant at 35 N, and finally a sine wave, whose mean value linearly decreases down to 15 N, of amplitude 8 N and frequency 1.5 Hz, chosen as in (Puricelli et al., 2023) for a fair comparison.

The ACMPFC performances are placed in opposition to two other force control strategies, already compared to each other in (Puricelli et al., 2023): one is based on classical control theory, i.e. a Proportional-Integral Force Controller (PIFC) (Roveda and Piga, 2021), the other is based on a pre-trained NNs ensemble (ORACLE) (Puricelli et al., 2023). Both control approaches are configured with the same parameters as proposed in (Puricelli et al., 2023).

3.2 Implementation Setup

All the modules involved in the architecture shown in Figure 2 interface with each other via ROS (Robot Operating System) communication mechanisms. They are developed in Python3, with the NNs

[1]https://youtu.be/7ysG4lz5lVY

[2]https://github.com/unisa-acg/actor-critic-model-predictive-force-controller

Table 1: Hyperparameters for ACMPFC NNs: *depth* indicates the number of fully-connected layers, *width* indicates the number of neurons per layer

Parameter	Actor	Critic	MA
Depth	2	2	3
Width	200	128	300
Learning rate	1e−4	1e−4	1e−3
Optimizer	Adam	Adam	Adam
Loss function	MSE	MSE	MSE
Dropout probability	0.1	0.1	0.2
Activation function	ReLU	ReLU	ReLU

Table 2: Impedance control parameters along the z axis

Environment	M_{imp} [kg]	ξ	K_{imp} [N/m]
Simulated	8	1.42	12000
Real	10	1.42	10500

Table 3: MSE [N^2] comparison between the PIFC (Roveda and Piga, 2021), the ORACLE (Puricelli et al., 2023) and the ACMPFC (ours), with force control active only along the z axis.

Environment	PIFC	ORACLE	ACMPFC
Simulated	8.16	1.55	3.07
Real	9.62	3.45	2.21

implemented through the PyTorch framework (Paszke et al., 2019). The discount factor in (2) is set to $\lambda = 0.95$, while the coefficients of the reward function (3) are chosen as $c_0 = 1$ and $c_1 = 2$. The parameters for the CEM are $T = 5$, $N_{it} = 3$, $N_{samples} = 128$, $N_{elites} = 4$, and $\alpha = 0.95$ (see Algorithm 1).

As regards the NNs design, their hyperparameters are listed in Table 1. In particular, the model approximator column refers to the values of the 3 base estimators of the ensemble. An exponential epoch-based scheduler is applied to the learning rate to improve the training speed.

The low-level impedance controller is tuned following the principles of (Roveda and Piga, 2021); the resulting parameters are listed in Table 2, which solely reports the gains for the z axis since it is the only direction of interest for the polishing-like task considered in this work.

3.3 Simulation results

As mentioned in Section 3.1, the simulation setup is set to mimic the real environment of Figure 1 exploiting the Robosuite framework (Zhu et al., 2020) to control the virtual robot in the MuJoCo simulator (Todorov et al., 2012). The manipulator is commanded via the control scheme of Figure 2, whose control loop frequency is set at 1 kHz.

The robot, during the execution of a trajectory, slowly approaches the table and, once the contact is established, the high-level force control loop is activated. The gains of the base PIFC are $K_P = 0.0008\,\mathrm{m/N}$ and $K_I = 0.008\,\mathrm{s\,m/N}$.

The simulation results are collected in Table 3: after convergence, the ACMPFC strategy improves the performances compared to the PIFC, while they are slightly worse than ORACLE. The force-tracking MSE $= (f_d - f_e)^2$ is computed on the reference trajectory described in Section 3.1.

As regards training and convergence, 10 episodes are needed to reach a stable MSE in tracking. Each reference trajectory takes 30 seconds and, between episodes, the NNs training time takes, on average, ca. 60 seconds. These times are achieved on a configuration composed of an i5-7300HQ CPU, GTX1050Ti GPU (Mobile), and Ubuntu 20.04.

3.4 Experimental results

In the real scenario, a thin block is placed onto a larger and stiffer thin layer, sliding over the table, and dragged by the robot during motion. Figure 1 displays the experimental configuration. The parameters are the same as those in Section 3.2, while the PIFC's parameters are, as in (Puricelli et al., 2023), $K_P = 0.001\,\mathrm{m/N}$ and $K_I = 0.008\,\mathrm{s\,m/N}$.

As reported in Table 3, the real-world experiments confirm a performance improvement for the force

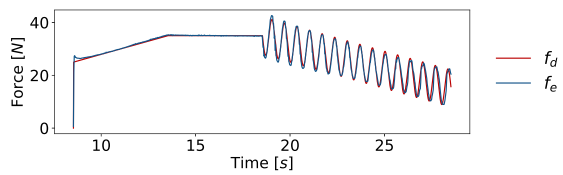

(a) Training trajectory

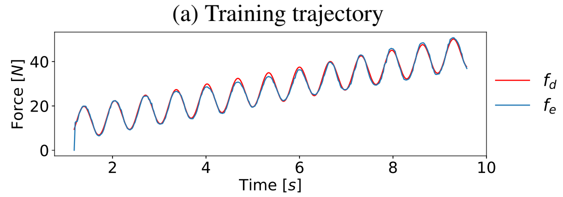

(b) Test trajectory

Figure 3: ACMPFC force tracking along z direction in the real scenario after convergence.

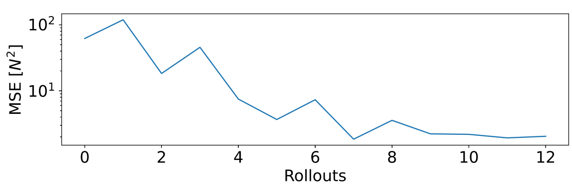

Figure 4: ACMPFC Mean Squared Error trend evolution over the training episodes. Force tracking is active only along the z direction. Convergence is reached after the 10$^{\text{th}}$ episode.

profiles under test, plotted in Figure 3. In fact, once convergence is reached (around the 10^{th} episode, as shown in Figure 4), the MSE obtained by the PIFC (Roveda and Piga, 2021) is reduced by a factor of 4.35; also, compared to the ORACLE learning-based strategy (Puricelli et al., 2023), our ACMPFC further reduces the MSE by a factor of 1.56.

It can be noticed that the MSE is high at the beginning of the training process, since the Actor behaves almost randomly (in the limited action range, as specified in Section 2.3.4), and decreases exponentially as the rollouts progress, demonstrating the effectiveness of the Actor-Critic RL strategy. The evident non-monotonic trend might be avoided by lowering the NN's learning rate; however, this would require more rollouts for convergence. Thus, the MSE trend is justified by jumps in the action's policy space during the Actor's training throughout the episodes. The effect of the convergent phenomenon can be better visualized in Figure 5: it is immediate to deduce that, as the rollouts advance, the exerted force profile tends to the desired one, proving that the Actor's policy converges to the optimal one.

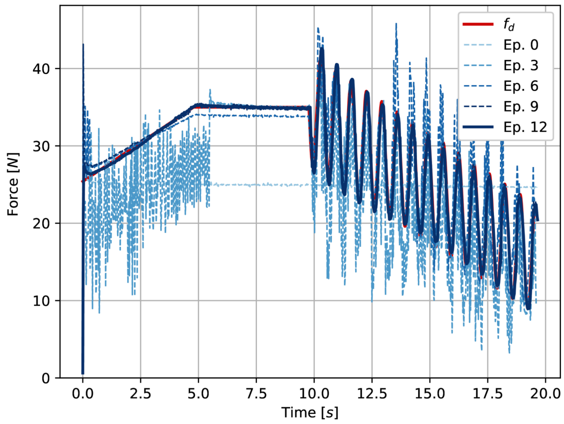

Figure 5: Exerted force over the episodes: throughout the rollouts, the actual force tends to the desired force, demonstrating the convergence of the Actor's policy to the optimal one.

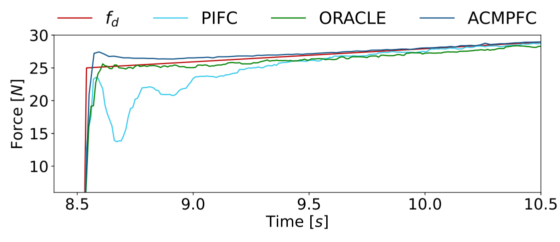

(a) Contact phase

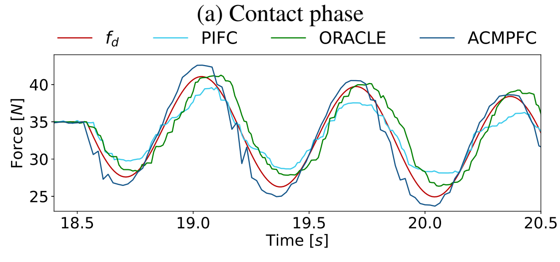

(b) Sine wave

Figure 6: Force tracking at some critical points. Three control strategies are compared: PIFC (Roveda and Piga, 2021), ORACLE (Puricelli et al., 2023), and ACMPFC (ours).

Figure 6 shows the performance of the three different strategies at particular points of the trajectory. The ACMPFC is able to track the reference, with overshoots of ca. 2 N during the initial contact and sine peaks. However, the ACMPFC strategy, compared to ORACLE (Puricelli et al., 2023), does not present any delay in tracking the desired force profile (as evident from Figure 6b), thus its performances in terms of MSE are in general better, as quantitatively confirmed by the results in Table 3.

Finally, the fact that the system is capable of tracking force references accurately, by efficiently learning the interaction dynamics, is proven by asking the robot to perform a validation trajectory, different than the training one. The training trajectory is that of Figure 3a, while the system's performance on the validation trajectory is reported in Figure 3b; in the latter, $\text{MSE} = 2.73\,\text{N}^2$ is achieved, which is comparable to the result obtained on the former.

4 CONCLUSIONS

This work proposes an Actor-Critic Model-Predictive Force Controller (ACMPFC), adapting and validating an already existing methodology (Roveda et al., 2022) in a context of accurate force tracking, i.e. extending its scope from human-robot collaboration to robot-environment interaction. The strategy is composed of two control loops: a low-level Cartesian impedance controller, and a high-level NN-based controller, whose inference optimizes the impedance controller's setpoint, allowing for accurate force tracking when performing a contact task in an unknown environment.

The NNs constituting the high-level controller are trained according to a RL-based approach. An Actor-Critic learning strategy computes optimal actions by making use of a model approximator, i.e. a NN ensemble modeling the robot-environment interaction dynamics.

The ACMPFC is tested both through MuJoCo simulations and in a real scenario, proving capable of overcoming the performance of a PI direct force controller (Roveda and Piga, 2021) and the AI-based

ORACLE strategy (Puricelli et al., 2023), in terms of force-tracking MSE, while achieving fast convergence.

Future work could be devoted to the employment of the proposed strategy in higher-dimensional tasks.

REFERENCES

Ataşlar-Ayyıldız, B. (2023). Robust Trajectory Tracking Control for Serial Robotic Manipulators Using Fractional Order-Based PTID Controller. *Fractal and Fractional*, 7(3):250.

Bellman, R. (1952). On the Theory of Dynamic Programming. *Proceedings of the National Academy of Sciences*, 38(8):716–719.

Bellman, R. (1958). Dynamic programming and stochastic control processes. *Information and Control*, 1(3):228–239.

Chua, K., Calandra, R., McAllister, R., and Levine, S. (2018). Deep Reinforcement Learning in a Handful of Trials using Probabilistic Dynamics Models. In *Proc. Adv. Neural Inform. Process. Syst.*, volume 31, pages 4754–4765.

de Boer, P.-T., Kroese, D. P., Mannor, S., and Rubinstein, R. Y. (2005). A Tutorial on the Cross-Entropy Method. *Annals of Operations Research*, 134:19–67.

Duan, J., Gan, Y., Chen, M., and Dai, X. (2018). Adaptive variable impedance control for dynamic contact force tracking in uncertain environment. *Robot. Auton. Syst.*, 102:54–65.

Formenti, A., Bucca, G., Shahid, A. A., Piga, D., and Roveda, L. (2022). Improved impedance/admittance switching controller for the interaction with a variable stiffness environment. *Complex Eng. Syst.*, 2(3):12.

Fujimoto, S., van Hoof, H., and Meger, D. (2018). Addressing Function Approximation Error in Actor-Critic Methods. *arXiv preprint*.

Haarnoja, T., Zhou, A., Abbeel, P., and Levine, S. (2018). Soft Actor-Critic: Off-Policy Maximum Entropy Deep Reinforcement Learning with a Stochastic Actor. *arXiv preprint*.

Hogan, N. (1984). Impedance Control: An Approach to Manipulation. In *Proc. Amer. Contrl. Conf.*, pages 304–313, San Diego, CA, USA.

Iskandar, M., Ott, C., Albu-Schäffer, A., Siciliano, B., and Dietrich, A. (2023). Hybrid Force-Impedance Control for Fast End-Effector Motions. *IEEE Robotics and Automation Letters*, 8(7):3931–3938.

Johannink, T., Bahl, S., Nair, A., Luo, J., Kumar, A., Loskyll, M., Ojea, J. A., Solowjow, E., and Levine, S. (2019). Residual Reinforcement Learning for Robot Control. In *Proc. IEEE Int. Conf. Robot. Autom.*, pages 6023–6029, Montreal, QC, Canada.

Jung, S., Hsia, T. C. S., and Bonitz, R. G. (2004). Force Tracking Impedance Control of Robot Manipulators Under Unknown Environment. *IEEE Trans. Control Syst. Technol.*, 12(3):474–483.

Kasruddin Nasir, A. N., Ahmad, M. A., and Tokhi, M. O. (2021). Hybrid spiral-bacterial foraging algorithm for a fuzzy control design of a flexible manipulator. *Journal of Low Frequency Noise, Vibration and Active Control*, 41(1):340–358.

Khatib, O. (1987). A unified approach for motion and force control of robot manipulators: The operational space formulation. *IEEE J. Robot. Autom.*, 3(1):43–53.

Lee, K.-k. and Buss, M. (2008). Force Tracking Impedance Control with Variable Target Stiffness. *IFAC Proc. Vol.*, 41(2):6751–6756.

Li, K., He, Y., Li, K., and Liu, C. (2023). Adaptive fractional-order admittance control for force tracking in highly dynamic unknown environments. *Industrial Robot: the international journal of robotics research and application*.

Liang, X., Zhao, H., Li, X., and Ding, H. (2018). Force tracking impedance control with unknown environment via an iterative learning algorithm. In *Proc. IEEE 3rd Int. Conf. Adv. Robot. Mechatron.*, pages 158–164, Singapore, Singapore.

Lillicrap, T. P., Hunt, J. J., Pritzel, A., Heess, N., Erez, T., Tassa, Y., Silver, D., and Wierstra, D. (2015). Continuous control with deep reinforcement learning. *arXiv preprint*.

Liu, Y., Jiang, D., Yun, J., Sun, Y., Li, C., Jiang, G., Kong, J., Tao, B., and Fang, Z. (2022). Self-Tuning Control of Manipulator Positioning Based on Fuzzy PID and PSO Algorithm. *Frontiers in Bioengineering and Biotechnology*, 9.

Mason, M. T. (1981). Compliance and Force Control for Computer Controlled Manipulators. *IEEE Trans. Syst. Man Cybern.: Syst.*, 11(6):418–432.

Mohd Hanif, M. I. F., Ahmad, M. A., and Jui, J. J. (2021). PID Tuning Method Using Chaotic Safe Experimentation Dynamics Algorithm for Elastic Joint Manipulator. *Journal Européen des Systèmes Automatisés*, 54(5):693–698.

Nagabandi, A., Kahn, G., Fearing, R. S., and Levine, S. (2018). Neural Network Dynamics for Model-Based Deep Reinforcement Learning with Model-Free Fine-Tuning. In *Proc. IEEE Int. Conf. Robot. Autom.*, Brisbane, QLD, Australia.

Obadina, O. O., Thaha, M. A., Mohamed, Z., and Shaheed, M. H. (2022). Grey-box modelling and fuzzy logic control of a Leader–Follower robot manipulator system: A hybrid Grey Wolf–Whale Optimisation approach. *ISA Transactions*, 129:572–593.

Paszke, A., Gross, S., Massa, F., Lerer, A., Bradbury, J., Chanan, G., Killeen, T., Lin, Z., Gimelshein, N., Antiga, L., Desmaison, A., Köpf, A., Yang, E., DeVito, Z., Raison, M., Tejani, A., Chilamkurthy, S., Steiner, B., Fang, L., Bai, J., and Chintala, S. (2019). PyTorch: An Imperative Style, High-Performance Deep Learning Library. In *Proc. Adv. Neural Inform. Process. Syst.*, Red Hook, NY, USA. Curran Associates Inc.

Peng, G., Philip Chen, C. L., He, W., and Yang, C. (2021). Neural-Learning-Based Force Sensorless Admittance Control for Robots With Input Deadzone. *IEEE Trans. Ind. Electron.*, 68(6):5184–5196.

Preitl, Z., Precup, R.-E., Tar, J. K., and Takács, M. (2006). Use of multi-parametric quadratic programming in fuzzy control systems. *Acta Polytechnica Hungarica*, 3(3):29–43.

Puricelli, L., Pozzi, A., Petrone, V., Ferrentino, E., Chiacchio, P., Braghin, F., and Roveda, L. (2023). Optimized Residual Action for Interaction Control with Learned Environments. *TechRxiv Preprint*.

Rigatos, G., Siano, P., Selisteanu, D., and Precup, R.-E. (2016). Nonlinear Optimal Control of Oxygen and Carbon Dioxide Levels in Blood. *Intelligent Industrial Systems*, 3(2):61–75.

Roveda, L., Castaman, N., Franceschi, P., Ghidoni, S., and Pedrocchi, N. (2020). A Control Framework Definition to Overcome Position/Interaction Dynamics Uncertainties in Force-Controlled Tasks. In *2020 IEEE International Conference on Robotics and Automation (ICRA)*, pages 6819–6825.

Roveda, L. and Piga, D. (2021). Sensorless environment stiffness and interaction force estimation for impedance control tuning in robotized interaction tasks. *Auton. Robots*, 45(3):371–388.

Roveda, L., Testa, A., Shahid, A. A., Braghin, F., and Piga, D. (2022). Q-Learning-based model predictive variable impedance control for physical human-robot collaboration. *Artificial Intelligence*, 312:103771.

Sathish Kumar, A., Naveen, S., Vijayakumar, R., Suresh, V., Asary, A. R., Madhu, S., and Palani, K. (2023). An intelligent fuzzy-particle swarm optimization supervisory-based control of robot manipulator for industrial welding applications. *Scientific Reports*, 13(1):8253.

Seraji, H. and Colbaugh, R. D. (1997). Force Tracking in Impedance Control. *Int. J. Robot. Res.*, 16(1):97–117.

Shu, X., Ni, F., Min, K., Liu, Y., and Liu, H. (2021). An Adaptive Force Control Architecture with Fast-Response and Robustness in Uncertain Environment. In *Proc. IEEE Int. Conf. Robot. Biomim.*, pages 1040–1045, Sanya, China.

Todorov, E., Erez, T., and Tassa, Y. (2012). MuJoCo: A physics engine for model-based control. In *Proc. IEEE Int. Conf. Intell. Robots Syst.*, pages 5026–5033, Vilamoura-Algarve, Portugal. IEEE.

Ucgun, H., Okten, I., Yuzgec, U., and Kesler, M. (2022). Test Platform and Graphical User Interface Design for Vertical Take-Off and Landing Drones. *Romanian Journal of Information Science and Technology*, 25(3–4):350–367.

Zhang, X., Sun, L., Kuang, Z., and Tomizuka, M. (2021). Learning Variable Impedance Control via Inverse Reinforcement Learning for Force-Related Tasks. *IEEE Robot. Autom. Lett.*, 6(2):2225–2232.

Zhu, Y., Wong, J., Mandlekar, A., Martín-Martín, R., Joshi, A., Nasiriany, S., and Zhu, Y. (2020). robosuite: A Modular Simulation Framework and Benchmark for Robot Learning. *arXiv preprint*.